

<https://doi.org/10.21608/sjsci.2023.183901.1054>

Studying the Characteristics and Performance of a New Heterogeneous Catalyst Pre-templated Using Cu(II) Schiff Base Complex on reducing 4-nitrophenol.

Laila H. Abdel-Rahman^{a,*}, Khaled M. H. Mohammed^{a,b}, Ebtehal Abdel-Hameed Ahmed^a, Salah F. Alzarzah^a, and Ayman Nafady^{a,c}

^a Chemistry Department, Faculty of Science, Sohag University, Sohag 82524, Egypt.

^b School of Chemistry, University of Southampton, Southampton, SO17 1BJ, UK.

^c Chemistry Department, College of Science, King Saud University, Riyadh, 11451, Saudi Arabia.

*E-mail: laila.abdelrahman@science.sohag.edu.eg

Received: 14th January 2023, Revised: 27th February 2023, Accepted: 11th March 2023

Published online: 15th March 2023

Abstract: The conversion of nitro compounds to their corresponding amino compounds by reduction route is a significant chemical reaction from an industrial and environmental standpoint. In the present paper, copper Schiff base complex was successfully prepared from the reaction between (1, 1'-(pyridine- 2,3- dimethyl imino methyl)naphthalene-2,2' -diol) and Cu(CH₃COO)₂ salt. This was successfully characterized with different techniques and grafted over graphene oxide (GO) as support after functionalizing it via chemical grafting using aminopropyltriethoxysilane (APTES) as a linker to obtain the functionalized form (FGO). The new heterogeneous complex (CuMGO) was depicted using physicochemical and spectroscopic tools such as FT-IR, UV-Vis, SEM, XRD, Raman spectroscopy, and XPS. The results manifest that Cu(II) imine complex was successfully immobilized on GO. The resulting catalyst was used to reduce 4-nitrophenol (4-NP) to its corresponding amine 4-aminophenol (4-AP) at room temperature in case of using hydrazine hydrate as a reducing agent. It showed good activity with a percent of conversion (44.4%) and an apparent rate constant of $2.06 \times 10^{-3} \text{ min}^{-1}$ in about 130 min. The prepared catalyst can be recycled five times without losing its activity.

Keywords: Cu(II) complex, Graphene oxide, catalytic reduction, 4-nitrophenol, XRD, SEM, Schiff base.

1. Introduction

Imine ligands are multilateral compounds that can be used over a wide area as chelating agents in coordination chemistry because they can form highly stable transition metal complexes. Reported studies show that Schiff's bases and their complexes can be applied in multiple domains, such as catalysis [1, 2], luminescence [3], and antimicrobial activities [4-6]. Imine metal complexes are effective catalysts in either homogeneous or heterogeneous processes, and the overall catalytic efficiency depends on the type of imine, the coordinated active sites, and the metal ions used [7, 8]. Recently, a number of homogeneous catalyst structures for the synthesis of amines by reduction of nitro groups have been reported [9, 10]. Cu(II) complexes of the Schiff base ligands have great importance as active homogeneous catalysts in oxidation reactions, synthesis reactions, and in the reduction of organic compounds [11]. However, these homogeneous systems face challenges when they are industrially and pharmaceutically applied, owing to high costs of preparation, product contaminants, and problems of separating the catalyst from the reaction medium [12]. Conversely, the need to develop new structures that are highly active and easily separable is being explored. This can be completed by immobilizing a complex of Schiff's bases on the solid surface for supporting and developing efficient heterogeneous catalysts [13]. Many studies were conducted to effectively immobilize

transition metals on several stable solid supports such as mesoporous silica [14], zeolites [15], clays [16], collagen fibers [17], boehmite [18], metal-organic frameworks (MOFs) [19], and carbonaceous nanomaterials [20, 21].

In particular, carbonaceous materials have improved versatility in catalysis. Graphene oxide, a two-dimensional sp²-hybrid carbon nanomaterial, has remarkable properties, including a large surface area, hydroxyl and carboxyl moieties, abundant hydrophilic epoxides, and greater mechanical energy and flexibility [22]. All graphene oxide-based materials have the potential to significantly improve a wide range of applications, including sensors, composite materials, catalysis, solar cells, and fuel storage [23]. GO-based catalysts are heterogeneous catalysts that can be used to classify a variety of financial and ecological challenges because of their exquisite synergism [24]. For example, Li et al. [25] have demonstrated that Cu(II) and Co(II) Schiff base complexes immobilized on GO showed higher conversion and selectivity for aerobic epoxidation of styrene. Furthermore, they were easily recovered and could be recycled many times without losing their activity. Rahmatpour et al. [26] have recently reported the immobilization of Cu(II) Schiff base complex on Fe₃O₄ nanoparticles as an active nanocatalyst for 2-amino-4 H benzo[h]chromenes and the reduction of 4-nitrophenol. The prepared catalyst was recovered and reused over 4 cycles with no significant decrease of its activity. Moreover, Dastjerdy et al. [27] prepared a copper complex immobilized on magnetic

GO as a heterogeneous catalyst for treating environmental pollutants and preparing chromenes. It can be considered chemically stable and could be recycled without loss of activity. A copper complex bearing 5-amino-tetrazole ligand onto graphene oxide nanosheets was synthesized. The catalytic activity of the prepared catalyst was evaluated in 4-nitrophenol (4-NP), methylene blue (MB), Rhodamine B (RhB), nigrosin (NS), and congo red (CR) reduction with NaBH₄. The catalyst showed high recyclability for six cycles [28].

Nitro aromatics are among the most important and largest chemicals in use today. It is surprisingly uncommon in nature and is mostly created by human activity. The US Environmental Protection Agency has classified it as a hazardous contaminant due to environmental hazards. As a result, the development of a methodology for conversion to harmless nitroamines has become a top priority and an essential focus for environmental protection [29]. However, the catalytic reduction of nitroaromatics is considered an essential chemical reaction in the fabrication of many compounds, including dyes, the pharmaceutical industry, and the production of pesticides [30-33]. Although many studies have been reported extending more environmentally friendly methods for the selective reduction of nitro compounds to their amino analogues [34, 35], Most of these methods have some limitations. Recent studies have extensively investigated the conversion of 4-NP to 4-AP by sodium borohydride as a hydrogen source [36]. However, little is known in the literature about using hydrogen sources other than sodium borohydride, particularly aqueous hydrazine, for 4-NP reduction. Aqueous hydrazine, a hydrogen storage material that contains no carbon atoms, has some worthy characteristics as it exists in a liquid form in a wide range of temperatures [37]. It is also significantly less expensive than sodium borohydride and formic acid (7 times and 1.4 times the Sigma-Aldrich price, respectively), and is relatively easy to manufacture. There has recently been renewed interest in using hydrazine hydrate as a hydrogen source to reduce 4-NP to 4-AP.

In this study, a novel catalyst has been successfully synthesized for the first time by immobilization of copper imine complex on GO using a simple and convenient method via surface functionalization with 3-APTES. The catalytic efficiency of the Schiff/GO-based Cu(II) catalyst was also investigated to reduce 4-NP to 4-AP under mild conditions in the existence of hydrazine hydrate as a hydrogen source. Also, we are interested in comparing the catalytic performance of the new heterogenized catalyst with its homogeneous template. We can successfully demonstrate that the presence of the Schiff base complex above the surface of GO adds characteristic properties and makes it an efficient catalyst. The advantages of the present system is derived from the properties of GO as well as the presence of a copper complex on the surface of GO, which is accountable of its catalytic behavior.

2. Experimental section

2.1. Materials and characterization devices

Chemicals were purchased from Sigma Aldrich or Merck and used without purification. The melting points were estimated on Gallenkamp (UK) apparatus. CHN analysis was collected using CHN-analyzer (Perkin-Elmer model 240c). FT-

IR spectra were done by (FT-IR Alpha Bruker with Platinum - Ate with KBr pellets) apparatus from 400 to 4000 cm⁻¹ with a resolution of 4 cm⁻¹. ¹HNMR with DMSO solvent was recorded using a Bruker Biospin NMR spectroscopy magnet device model 400 MHz. The molar conductance was measured by Jenway conductivity/TDS meter model 4510 in dimethylformamide solvent at room temperature and (1×10⁻³ M) of the complex. The UV-Vis spectra of the prepared compounds were performed using DMF as a solvent and scanned by PG spectrophotometer model T+80 at 298 K. For GO (2 mg) was taken and dissolved in DMF with sonication for about 10 minutes. Gouy's balance was utilized to evaluate the magnetic characteristics of the complex, and the calibration was performed by diamagnetic corrections, which resulted from Pascal's constants and Hg[Co(SCN)₄]. Bruker D8 Advance using monochromatic Cu- α radiation ($k = 1.5406 \text{ \AA}$) was used to perform X-ray powder diffraction analysis. SEM analysis was conducted via QUANTA FEG250 at the National Research Center, Egypt. Raman spectroscopic analysis was carried out through WI Tec alpha 300 RA. XPS was calculated on K-ALPHA (Thermo Fisher Scientific, USA) with monochromatic X-ray Al K-alpha radiation -10 to 1350 e.v spot size 400 micro m at pressure 10-9 m bar with full spectrum pass energy 200 e.v and at a narrow spectrum of 50 eV. The UV-Vis scan of the reduction was recorded on PG spectrophotometer model T+80 at 298 K in the range 200 nm to 600 nm.

2.2. Synthesis

2.2.1. Synthesis of graphene oxide and its amino functionalized form

A modified Hummer method was utilized to synthesize GO [38]. In an unconventional experiment, 2.0 g of graphite powder and concentrated H₂SO₄ (46 ml) were put together in a 250 ml flask. Within 2 hours, the resulting mixture was cooled to 0° C. while stirring in an ice bath. KMnO₄ (6 g) was added with robust stirring, and the flask was held at 0° C for 2 h for oxidation. The reaction solution was then stirred at 35 °C for 30 minutes. 96 ml of deionized water was added quietly to the reaction and increased the temperature to 95 °C over 15 minutes using an oil bath. The final step was accomplished by treating it with 30% H₂O₂ and 240 ml of deionized water [39]. Furthermore, the produced precipitate was filtered, and 5% HCl and deionized water was used for washing it until reaching pH = (4-5) [40]. Finally, the resulting material was dried at 70 °C for 3 days to obtain GO. The graphene oxide surface was functionalized with a slight modification of a known chemical grafting method. This experiment includes refluxing 0.5 g of GO with 7 ml of (3-APTES) dissolved in 15 ml dry toluene at 90°C for 4 h.

The formed solid was filtered and rinsed via toluene several times and dried overnight [41].

2.2.2. Synthesis of the imine ligand and its Cu(II) complex

To prepare the imine ligand, mix 0.545 g of pyridine 2, 3-diamine (5 mmol) with 1.72 g of 2-hydroxynaphthaldehyde (10 mmol) in ethyl alcohol (30 ml). The reaction was left for 30 min at 50 °C with stirring and piperidine drops added as a catalyst [42]. The yellow product was separated by filtration and washed with ethanol; it was dried over anhydrous CaCl₂.

Yellow color; m.p 260 °C; yield (87%). The Cu complex was synthesized by combining (2.08 g, 5 mmol) of the Schiff base and copper acetate monohydrate (0.99 g, 5 mmol) in 20 ml ethanolic solution. The mixture was left on the stirrer for 3 hours at 25 °C. The product was isolated and filtered. Ethanol was used for washing the precipitate before drying it in a vacuum with anhydrous calcium chloride.

2.2.3. Immobilization of the prepared complex on graphene oxide

A suitable amount of GO (0.1g) was dispersed in 10 ml of toluene using ultrasonication. The dispersed solution was added to (0.1 g, 10 ml toluene) of Cu(II) complex with 0.5 ml of Et₃N [43]. The reaction solution was stirred and refluxed at 50 °C for 5 h. The solid was collected via filtration, washed with toluene to remove the unreacted moieties, and left to dry.

2.3. Reduction of 4-NP

An aqueous and fresh solution of NH₂.NH₂.H₂O (1 ml, 10 mM) was added to a solution of 4-NP (0.1 mM, 3 ml) in a cuvette of quartz with a 1.0 cm path length. The color of the solution changed instantly to a deep-yellow color. 5 mg was added to the mixture, and the initial yellow color of the solution changed to colorless as the reaction proceeded. UV-Vis spectroscopy was used to follow the progress of the reaction.

3. Results and discussion

3.1. ¹HNMR of the prepared imine ligand

The prepared imine ligand displayed two singlet signals at (9.81 and 10.03 ppm) which referred to the azomethine protons. Also, it showed another two singlet signals with higher values at (14.36 and 15.12 ppm) for two hydroxyl protons [44]. The aromatic protons appeared as multiple signals in the range of (6.92-8.69 ppm). The ¹HNMR of the Schiff base ligand is presented in Fig. 1.

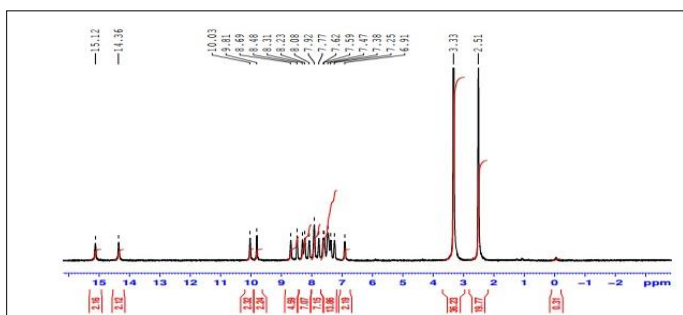


Fig. 1 shows the ¹HNMR spectrum of the prepared imine ligand.

3.2. Molar conductivity and magnetic properties of CuL

These analyses were performed to help in detecting the structural geometry of the prepared imine complex. The conductivity in DMF at [CuL] = 0.1 × 10⁻³ M was 11.50 μS, and the complex displayed a non-electrolytic nature [45]. Moreover, the magnetic properties were detected by evaluating the magnetic susceptibility of the prepared Cu(II) Schiff base complex and utilizing it in calculating the effective magnetic moment according to the following equation:

$$\mu_{\text{eff}} = 2.83\sqrt{Xm * T} \quad X'm = X_m - (\text{diamag. Corr.})$$

The results demonstrated that the CuL complex has paramagnetic properties with a 1.92 B. M value which agrees with an octahedral geometry [46].

3.3. IR spectra

The spectra of the prepared ligand exhibited a broad and medium band at 3427 cm⁻¹ that is assigned to the intramolecular hydrogen bonding the hydroxyl group [47]. The 1622 cm⁻¹ and 1562 cm⁻¹ correspond to the -C=N (imine and pyridine nitrogen) frequencies. On complexation, the imine band has a lower shift to 1603 cm⁻¹, suggesting the participation of the imine group in the formation of the complex [48, 49]. The pyridine nitrogen was still present at the same frequency, indicating that it doesn't coordinate with the metal ion. The broad band at 3373 cm⁻¹ in the spectrum of the complex is associated with coordinated water [50]. This was confirmed by a new and small band at 822 cm⁻¹. The -C-O band was found at 1349 cm⁻¹ which shifted to 1316 cm⁻¹ upon formation of the complex [51], confirming the presence of the phenolic oxygen in coordination with the metal ion. The appearance of new bands at 499 and 563 cm⁻¹ corresponds to the participation of N and O atoms in Cu(II) ions [52]. The IR spectra demonstrated that the ligand bonded to the metal ion via two imine nitrogens and two phenolic oxygens.

3.3. IR spectra

GO showed frequencies at 2797, 1709, 1612, 1222, and 1034 cm⁻¹, which were assigned to -CH, C=O, C=C, C-O, and C-O-C bonds, respectively [53]. For FGO spectrum, the bands that appeared at 3346 and 1559 cm⁻¹ indicate the presence of the (N-H) bond and confirm the successful functionalization of GO [54]. Also, two bands at 2867 and 2924 cm⁻¹ indicate the presence of aliphatic C-H moieties [55]. Compared to the previous, the azomethine linkage has a lower shift in CuMGO complex to 1602 cm⁻¹. The (N-H) frequencies were found at 3333 and 1534 cm⁻¹. In addition, the observation of a small and lower shift occurred to the M-O and M-N which appeared at 562 and 497 cm⁻¹, respectively can be retained to the effect of loading the complex to the surface of FGO and coordination of the complex to the surface of FGO via a propylamine linker. The spectra of the prepared compounds are presented in Table 1.

Table 1: IR spectra (cm^{-1}) of L, CuL, FGO, and CuMGO compounds.

Item	L	CuL	GO	FGO	CuMGO
$\nu(\text{OH})/\text{H}_2\text{O}$	3427	3373	3376		3464
$\nu(\text{C}=\text{N})$	1622	1603			1602
$\nu(\text{C-O-C})$			1222	1191	1250
C-O (epoxy)			1034	1092	1043
$\nu(\text{NH})$				3346/ 1559	3333/ 1534
$\nu(\text{Si-O-C})$				1006	981
$\nu(\text{M-O})$		563			562
$\nu(\text{M-N})$		499			497

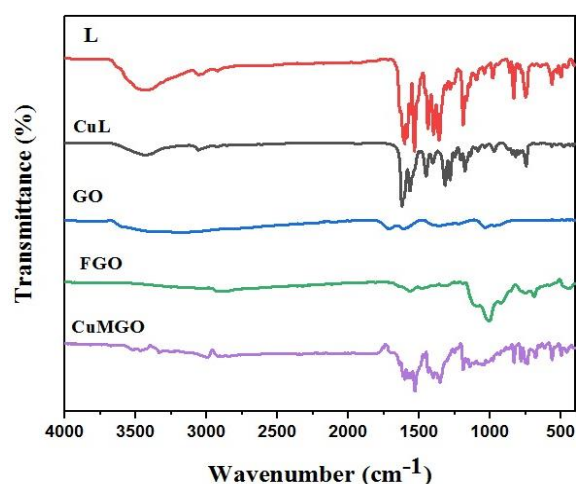


Fig. 2 IR spectra of the prepared compounds.

3.4. Molecular electronic spectroscopy

The UV-Vis scan of the free ligand shows two absorptions at 423 and 468 nm. The absorptions are associated with $\pi \rightarrow \pi^*$ and $n \rightarrow \pi^*$ transitions caused by the C=N moiety [56]. The corresponding spectrum of the complex possessed some bands at 330, 427, and 460 and a broad band at 619 nm. The first two transitions were assigned to $\pi \rightarrow \pi^*$ and $n \rightarrow \pi^*$, respectively. The other bands correspond to the LMCT band and d-d transitions. GO exhibited two characteristic bands at 238 and 284 nm, which referred to $\pi \rightarrow \pi^*$ transitions of C=C bonding and $n \rightarrow \pi^*$ for the transitions of the C=O group, respectively [57]. After immobilization, CuMGO displayed two bands at 327 and 350 nm related to $\pi \rightarrow \pi^*$ and $n \rightarrow \pi^*$ transitions. The d-d transitions were present at 430 and 465 nm. The results signify that a blue shift occurred in the case of an immobilized complex compared to the CuL Schiff base complex. This established that the metal Schiff base complex is strongly coordinated with the surface of amine-functionalized GO. The molecular electronic spectra are shown in **Fig. 3**.

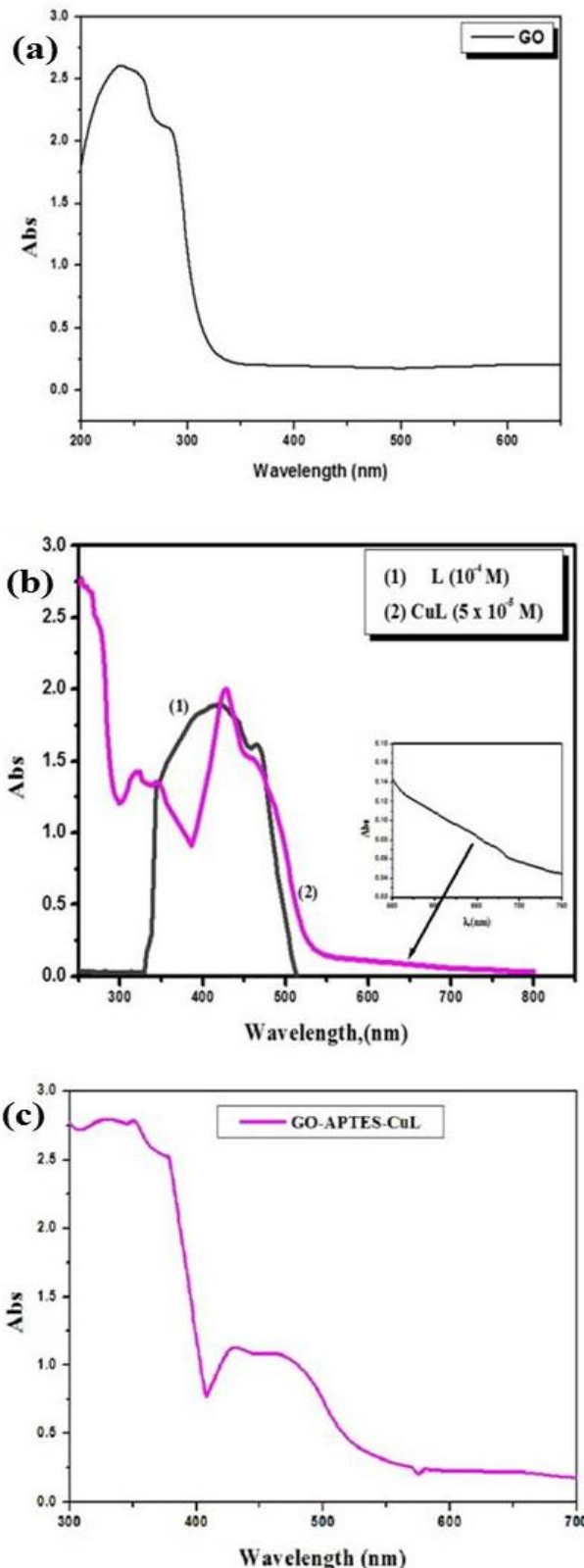


Fig. 3 Molecular electronic spectra of a) GO, b) (L and CuL) and c) GO-APTES-CuL.

3.5. Stoichiometric estimations.

A continuous variation method was carried out for confirming the stoichiometry of the synthesized imine complex [58, 59]. As seen in Fig. 4, the results confirmed the complex possesses a 1:1 mole ratio of the metal and ligand.

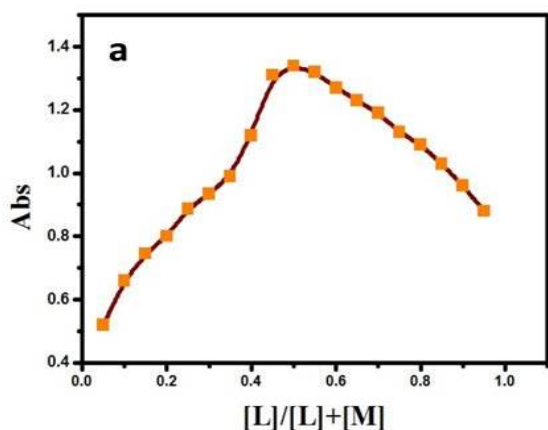


Fig. 4 Continuous variation for CuL complex in DMF at 298 K.

3.6. Elemental analyses of the prepared ligand and its Cu complex

The obtained imine ligand and complex were elucidated by (CHN) analyses. The results were compatible with the calculated values as listed in Table 2.

3.7. SEM and XRD analyses of GO, FGO and CuMGO.

The morphological features of the prepared catalyst were determined by SEM analysis. GO Fig (5.a) revealed a crumbled-layered structure with a smooth surface and thin layers like waves [60]. The results disclosed the microstructure and morphology of CuMGO (Fig. 5b). CuMGO also showed a disordered network with crumbling and an increase in the protrusion and roughness of the surface. The presented results confirmed the successful immobilization process. Fig. 6 depicts XRD patterns of GO, FGO, and CuMGO. Upon oxidation of graphite, a significant decrease was observed in the reference (002) peak of graphite at $\approx 26^\circ$ with a d-spacing of 0.34 nm [61]. On the other hand, GO displayed the characteristic (001) peak at $\approx 13^\circ$ with a d-spacing of 0.69 nm. The increase in the spacing between graphene oxide layers is attributed to the successful exfoliation of graphite and the insertion of oxygen-containing functional groups between the layers [62]. Moreover, loading APTES on GO decreased the intensity of the significant peak at 13° and the emergence of a broad peak at 22° . This is assigned to forming an amorphous silica layer indicating that GO oxygen-containing groups have been functionalized [63]. The characteristic peak of GO was shifted from 13° to 10° , corresponding to an increase of the d-spacing from 0.69 nm to 0.8 nm, indicating the presence of the imine complex on the surface of GO. This also implies that the GO structure was not destroyed during preparation [64]. The results indicate that CuMGO has an amorphous nature with a

broad peak at $\approx 25^\circ$ which is significant for the GO-based Schiff base complexes [65, 66]. The presence of small diffraction peaks in CuMGO pattern may be attributed to the loading of the pure imine complex on GO [67].

Table 2: Micro analytical and physical data of the Schiff base ligand and Cu(II) complex.

Compound	Empirical formula (molecular weight)	Color & Yield (%)	m.p. $^\circ\text{C}$	Elemental analysis (Calc%)			Molar conductance μS	μeff (B.M)
				Found	H	N		
L	$\text{C}_{27}\text{H}_{19}\text{N}_3\text{O}_2$ (417.49)	Yellow (87)	260	(77.60) 77.21	(4.55) 4.32	(10.06) 9.81		
CuL	$\text{C}_{27}\text{H}_{19}\text{N}_3\text{O}_2$ (417.49)	Yellow (87)	260	(77.60) 77.21	(4.55) 4.32	(10.06) 9.81	11.50	1.92

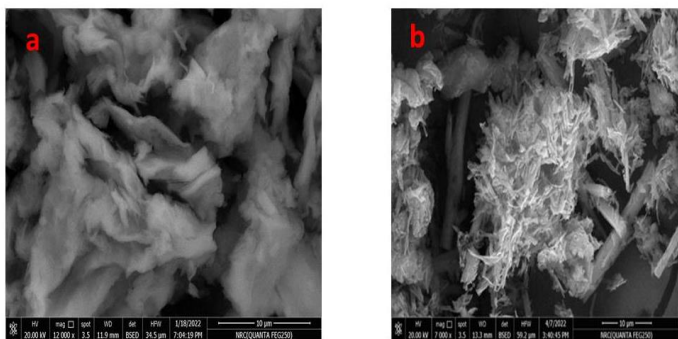


Fig. 5 SEM images for a) GO, b) CuMGO.

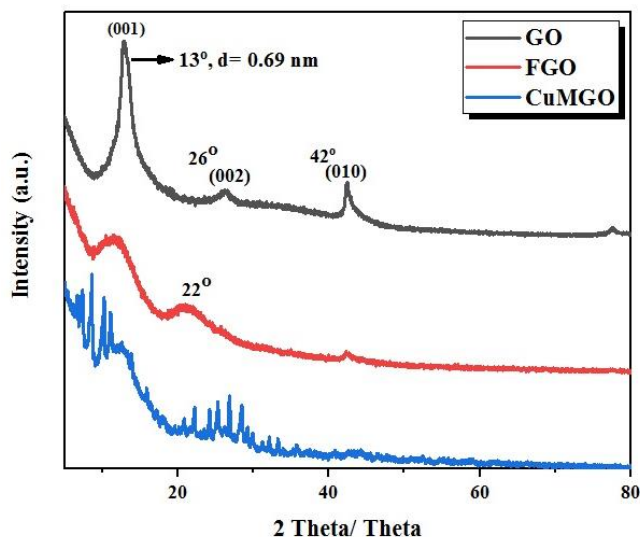


Fig. 6 XRD patterns for GO, FGO, and CuMGO.

3.8. Raman spectra

Fig.7 shows the Raman spectroscopy of GO, FGO, and CuMGO. The results showed two characteristic bands, D and G. The G band emerges by the vibrations of sp^2 carbon atoms, while D is assigned to the vibration of the sp^3 carbon atom. GO displayed two remarkable peaks at 1350 and 1600 cm^{-1} for D and G bands, respectively with I_D/I_G ratio of 0.88 [68]. The spectrum of FGO and CuMGO showed a lower shift for the D band, which appeared at 1345 and 1342 cm^{-1} , respectively. In contrast, the G band significantly shifted to 1608 and 1613 cm^{-1} for FGO and CuMGO. These findings support the occurrence of defects and disorder of the in-plane sp^2 domains. The (I_D/I_G) ratio increases to 1.011 for FGO and 1.03 for CuMGO compared with GO [69], which signifies that the functionalization of the surface of GO with CuL Schiff base complex increases the defect site and provides high catalytic performance.

3.9. XPS studies

XPS analyses were carried out to detect the oxidation state of Cu metal and The composition of elements of CuMGO. The survey spectrum is shown in Fig. 8a. Four peaks obviously appeared at 531.05 eV, 401.09 eV, 284.54 eV, and 104.24 eV referring to O, N, C, and Si, respectively [70]. Furthermore, the

core level of Cu2p (Fig. 8b) revealed the presence of two peaks with binding energies of 954.71 eV and 934.43 eV, confirming the Cu^{2+} oxidation state and agreeing well with the literature [71]. On the other hand, the Cu2p_{3/2} satellite peak was observed at 943.93 eV, indicating the attachment between the ligand and metal ion. XPS spectra of C1s possessed four characteristic peaks at 284.61, 286.04, 287.38, and 288.61 eV, which imputed to (C-H, C=C, C-C), (C-N, C-O), (C=N, C=O) and O-C=O, respectively [72]. The scan of the N1s region shows two peaks at 399.19 and 401.30 eV, which correspond to -C=N and -C-NH₂ nitrogen. FT-IR and XPS studies briefly revealed that an immobilized complex had been successfully prepared over the surface of amine-functionalized GO. The coordination of the imine ligand was stable without decomposition during the coordination to the functional group, as seen in Scheme 1.

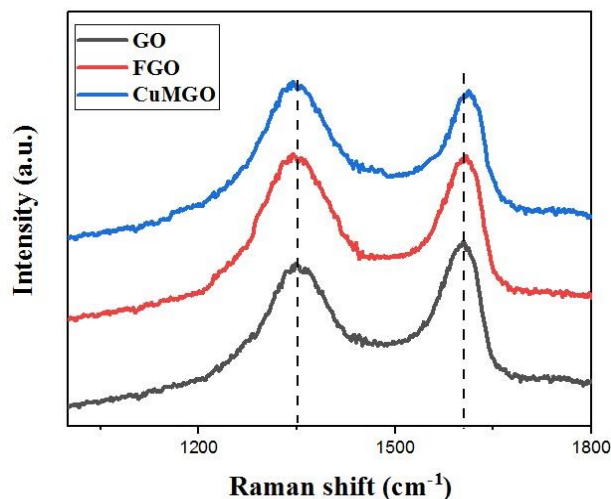


Fig. 7 Raman spectra of GO, FGO and CuMGO.

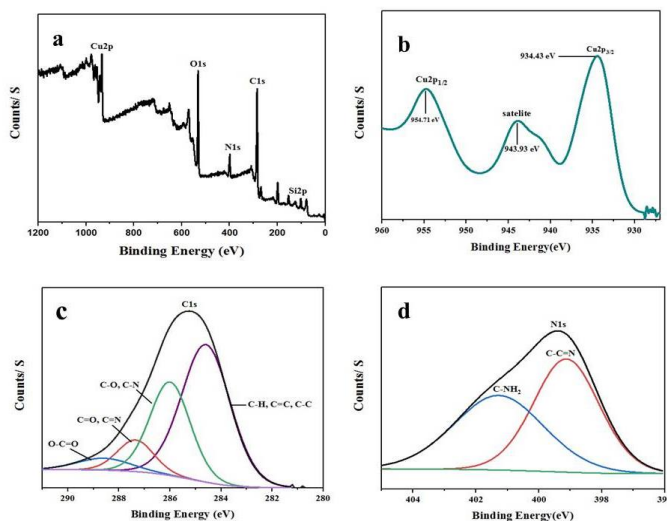
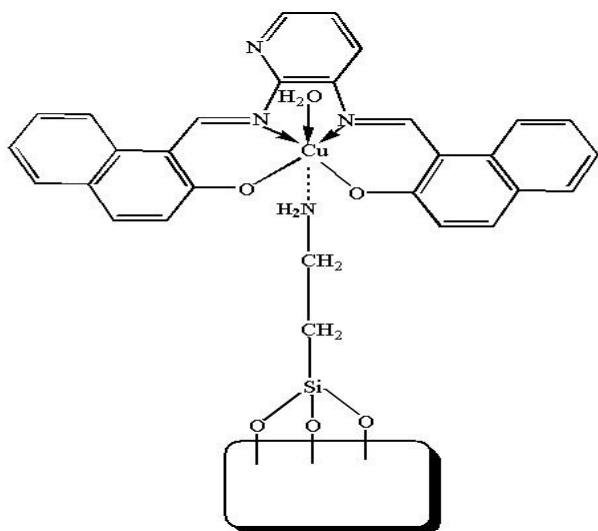


Fig. 8 The XPS spectra of CuMGO material for (a) full scan, (b) Core level, (c) C 1s and N 1s.



Scheme 1: The proposed structure for the prepared CuMGO catalyst.

3.10. Catalytic reduction of 4-NP.

The activity of the CuMGO catalyst in the reduction of 4-NP was investigated with the addition of an excess of $\text{NH}_2\text{NH}_2\cdot\text{H}_2\text{O}$. The reduction reaction was measured by UV-Vis spectra to follow the absorption decrease at $\lambda = 400$ nm, representing the absorption of the nitrophenolate ion. The UV-Vis spectrum of (0.1 mM) aqueous solution of 4-NP (**Fig. 9a**) displayed a maximum absorption peak at 316 nm. A red shift was observed upon adding $\text{NH}_2\text{NH}_2\cdot\text{H}_2\text{O}$. The shift was accompanied by a significant change in the solution's color from faint yellow to deep yellow with a maximum absorption of 400 nm (**Fig. 9b**), indicating the formulation of a 4-nitrophenolate (4-NP⁻) [73]. In the absence of the catalyst, there is no observable change in color, suggesting that $\text{NH}_2\text{NH}_2\cdot\text{H}_2\text{O}$ cannot reduce 4-NP ions by itself. The results implied that the CuMGO catalyst was the only one that converted 4-NP to 4-AP, while the GO and CuL complexes had no activity. (**Fig. 9c** and **Fig. 9d**).

The absorption of 4-NP was gradually reduced after adding a CuMGO catalyst (5 mg), whereas the intensity of a new absorption at 310 nm gradually increased [74, 75], indicating the formation of 4-AP. 4-NP was completely reduced in 130 minutes. The observation of the isosbestic point confirms that the conversion of 4-NP gives only one product, 4-AP [76, 77]. The catalytic performance was investigated in the presence of an excess of $\text{NH}_2\text{NH}_2\cdot\text{H}_2\text{O}$. As a result, the concentration of $\text{NH}_2\text{NH}_2\cdot\text{H}_2\text{O}$ was assumed to be constant throughout the reaction, and the rate constant (K_{app}) of the reaction was determined solely by the concentration of 4-NP. So, the results assumed that the first approximation is to fit the obtained data with the pseudo-first-order kinetics [78, 79]. The rate of reaction is calculated from the approximately linear fitting according to the following equation:

$$-k_{\text{app}} t = \ln (C_t/C_0) = \ln (A_t/A_0)$$

Where C_t and A_t represent the concentration and absorption of 4-NP at time (t) while C_0 and A_0 represent the concentration and absorption of 4-NP at the initial time of the reaction [80]. The slope of the relationship between $\ln (A_t/A_0)$ and the reaction time (t) was used to calculate the rate constant (k_{app}) as displayed in **Fig. 11a**. According to the fitted line, the rate constant was found to be $2.06 \times 10^{-3} \text{ min}^{-1}$ for 5 mg of catalyst. The concentration of 4-NP is proportional to the absorbance and (A_t/A_0) must equal (C_t/C_0) of 4-NP. The plot of (A_t/A_0) versus reaction time is shown in **Fig. 11b**. The obtained results for this relation were similar to the literature [81].

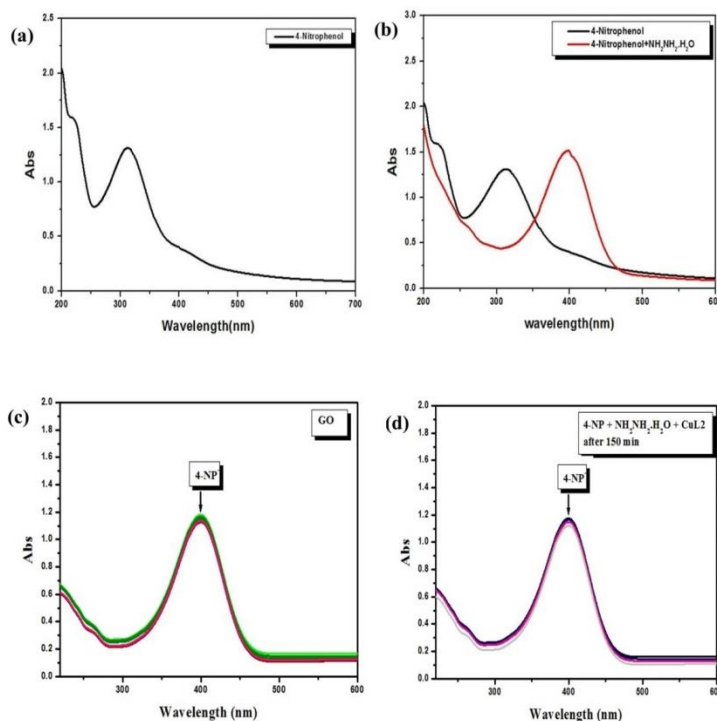


Fig. 9 UV-visible spectra in presence of (a) 4-NP (0.1 mM), (b) $\text{N}_2\text{H}_4\cdot\text{H}_2\text{O}$ (10 mM), (c) GO, and (d) CuL Schiff base complex at R.T.

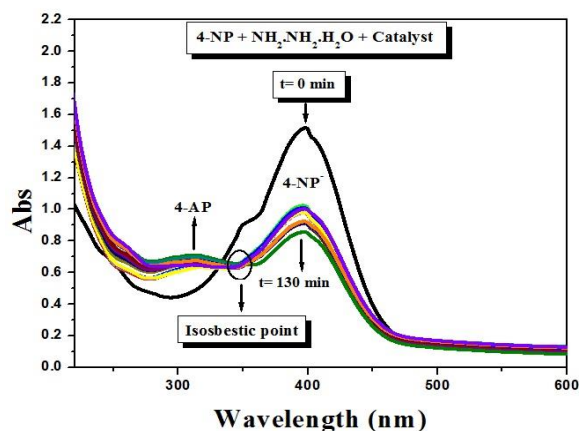
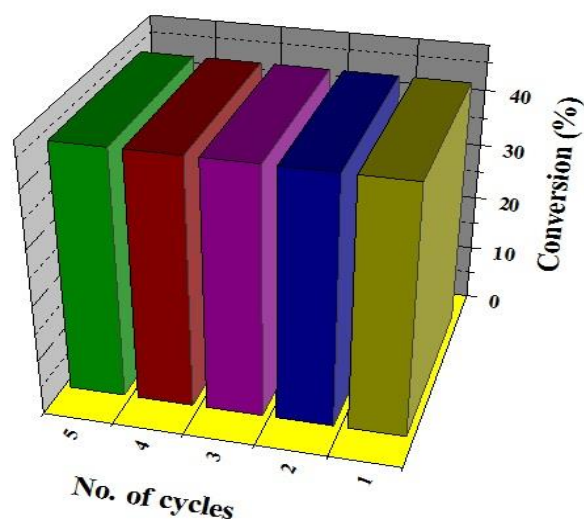


Fig. 10 UV-Vis scan of the reduction of 4-NP (0.1 mM) in presence of $\text{NH}_2\text{NH}_2\cdot\text{H}_2\text{O}$ (10 mM) and 5 mg of CuMGO catalyst.

The reaction's mechanism depends on the prepared catalyst's ability depends on the prepared catalyst's ability to provide an active surface for the reduction process to take place. The presence of hydrazine hydrate as a reaction component facilitates the formation of 4-NP⁻ ion as an intermediate. Thus, it increases the alkalinity which promotes the reduction process. Upon the catalyst's addition, hydrazine hydrate and 4-NP were adsorbed on its surface and catalytic reduction was initiated immediately by transferring the hydride from the hydrazine hydrate donor to the acceptor 4-NP. Finally, with the elimination of a molecule of H₂O, 4-AP departed the catalyst's surface [82]. The recyclability of the prepared catalyst was carried out five times by washing it multiple times with deionized water and reusing it for another cycle under the optimum conditions. The results revealed that the as-prepared catalyst could boost converting 4-NP to 4-AP five successive times with no discernible change in catalytic behavior Fig. 12.

The catalyst after recycling was investigated by FT-IR spectra and XRD analyses. The fresh catalyst and recycled one were identical in FT-IR, confirming that no significant changes occurred in the catalyst (Fig. 13a). Furthermore, comparing the XRD information of the fresh and recycled catalyst (Fig. 13b) shows that the XRD pattern of the recycled catalyst was kept during the recycling test. To investigate the advantages of the catalytic competence of the synthesized catalyst, the results of reducing 4-NP with different supported heterogeneous catalysts were listed in Table 3. As shown, the prepared catalyst showed good results with respect to others. The most advantages are the cheap and easy synthesis, using it at room temperature, and the short time compared to other catalysts under mild conditions.

in the presence of hydrazine hydrate at room temperature. It has shown a good performance (44.4%) when compared with CuL Schiff base complex, which gives zero activity. 5 mg of the prepared catalyst, has the ability to effectively reduce 4-NP and the reduction process was completed at 130 min with a reaction rate of $2.06 \times 10^{-3} \text{ min}^{-1}$. Moreover, the prepared catalyst was easily separated and recycled for multiple sequential runs. Based on the results, the synthesized catalyst offers satisfactory advantages such as ease of recovery and reuse, simple synthesis method, moderate conditions, low temperature, environmentally friendly solvents, and no use of



toxic substances.

Fig. 12 Recycling experiments with CuMGO for reduction of 4-NP. Optimum reaction conditions: 5 mg CuMGO; 4-NP (0.1 mM); NH₂NH₂.H₂O (10 mM); at room temperature; reaction time for run 130 min.

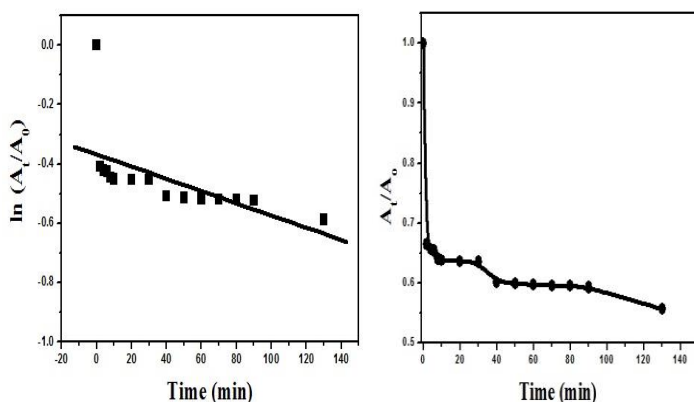


Fig. 11 The relation between (a) $\ln(A_t/A_0)$ and time and (b) A_t/A_0 vs time for the reduction of 4-NP to 4-AP over 5 mg CuMGO catalyst.

4. Conclusion

In summary, a new Cu(II) imine complex was successfully characterized and supported on the surface of functionalized GO. Several physicochemical, spectroscopic, and analytical tools were utilized for determining the structure of the synthesized catalyst including IR, UV-Vis, XRD, SEM, Raman spectroscopy, and XPS. The activity of the prepared catalyst (CuMGO) was tested by reducing 4-NP in an aqueous medium

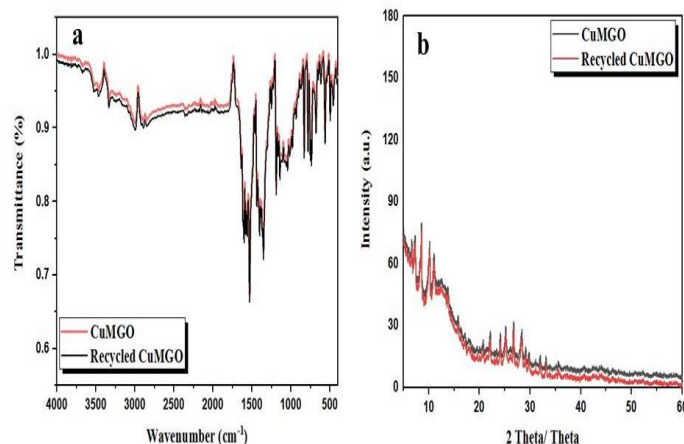


Fig. 13 Analyses of CuMGO and recycled CuMGO catalyst a) FT-IR spectra and b) XRD pattern.

Table 3: Comparison of the obtained results with those of a variety of supported catalysts for the reduction of 4-NP.

Catalyst name	Reducing agent	Time (min)	Temperature (°C)	Ref
p(AMPS)-Ni composite	NaBH ₄	330	Room temperature	[83]
GA-Pt NPs	NaBH ₄	480	Room temperature	[84]
Ru(II) complex/ZnO	NaBH ₄	1440	Room temperature	[85]
ZIS/rGO	NaBH ₄	180	Room temperature	[86]
Co/Al ₂ O ₃	NaBH ₄	180	Room temperature	[87]
hollow Pd nanocomposite	Hydrazine	150	80	[88]
RGO/Ni	NaBH ₄	140	Room temperature	[89]
CuMGO	Hydrazine	130	Room temperature	This work

References

- [1] M. Tümer, E. Akgün, S. Toroğlu, A. Kayraldiz, L. Dönbak, *Journal of Coordination Chemistry*, 61(18) (2008) 2935-2949.
- [2] X. Liu, C. Manzur, N. Novoa, S. Celedón, D. Carrillo, J.R. Hamon, *Coordination Chemistry Reviews*, 357 (2018) 144-172.
- [3] Z.Q. Feng, X.L. Yang, Y.F. Ye, *The Scientific World Journal*, 2013.
- [4] A. Palanimurugan, A. Kulandaisamy, *Journal of organometallic chemistry*, 861 (2018) 263-274.
- [5] E. Yousif, A. Majeed, K. Al-Sammarræ, N. Salih, J. Salimon, & B. Abdullah, *Arabian Journal of Chemistry*, 10 (2017) S1639-S1644.
- [6] M.A. Malik, O.A. Dar, P. Gull, M.Y. Wani, A.A. Hashmi, *MedChemComm*, 9(3) (2018) 409-436.
- [7] L.S. Ashoor, I.K. Mohaisen, R.K.R. Al-Shemary, *EurAsian Journal of BioSciences*, 14(2) (2020) 7541-7550.
- [8] A.M. Abu-Dief, I.M. Mohamed, *Beni-suef university journal of basic and applied sciences*, 4(2) (2015) 119-133.
- [9] G. Zhu, J. Geng, L. Yan, Y.K. Yuan, G.Z. Han, *Colloids and Surfaces A: Physicochemical and Engineering Aspects*, 580 (2019) 123697.
- [10] W.G. Jia, M. Li, X.T. Zhi, L.L. Gao, J. Du, *Journal of Molecular Structure*, 1217 (2020) 128349.
- [11] M.R. Maurya, A.K. Chandrakar, S. Chand, *Journal of Molecular Catalysis A: Chemical*, 274(1-2) (2007) 192-201.
- [12] P. Puthiaraj, W.S. Ahn, *Catalysis Communications*, 65 (2015) 91-95.
- [13] H. Hassan, A. Tolba, E.S. El-Sharkawy, *Frontiers in Scientific Research and Technology*, 1(1) (2020) 57-67.
- [14] C. Liu, R. Tan, N. Yu, D. Yin, *Microporous and mesoporous materials*, 131(1-3) (2010) 162-169.
- [15] K. Mori, Y. Miura, S. Shironita, H. Yamashita, *Langmuir*, 25(18) (2009) 11180-11187.
- [16] M. Ghiaci, F. Ansari, Z. Sadeghi, A. Gil, *Catalysis Communications*, 21 (2012) 82-85.
- [17] H. Wu, L. Zhuo, Q. He, X. Liao, B. Shi, *Applied Catalysis A: General*, 366(1) (2009) 44-56.
- [18] N.Y. Baran, T. Baran, M. Nasrollahzadeh, R.S. Varma, *Journal of Organometallic Chemistry*, 900 (2019) 120916.
- [19] C.K.P. Neeli, P. Puthiaraj, Y. R. Lee, Y.M. Chung, S.H. Baeck, W.S. Ahn, *Catalysis Today*, 303 (2018) 227-234.
- [20] B. Yoon, C.M. Wai, *Journal of the American Chemical Society*, 127(49) (2005) 17174-17175.
- [21] Y. Qu, T. Chen, G. Wang, *Applied Surface Science*, 465 (2019) 888-894.
- [22] M. Nasrollahzadeh, Z. Issaabadi, M.M. Tohidi, S.S. Mohammad, *The Chemical Record*, 18(2) (2018) 165-229.
- [23] H.P. Mungse, S. Verma, N. Kumar, B. Sain, O.P. Khatri, *Journal of materials chemistry*, 22(12) (2012) 5427-5433.
- [24] R. K. Sharma, S. Dutta, S. Sharma, R. Zboril, R.S., Varma, M.B. Gawande, *Green Chemistry*, 18(11) (2016) 3184-3209.
- [25] Z. Li, S. Wu, H. Ding, D. Zheng, J. Hu, X. Wang, Q. Kan, *New Journal of Chemistry*, 37(5) (2013) 1561-1568.
- [26] F. Rahmatpour, M. Kosari, N. Monadi, *Journal of Molecular Structure*, 1253 (2022) 132102.
- [27] M.S. Dastjerdy, N. Monadi, *Applied Organometallic Chemistry*, 37(1) (2023) e6931.
- [28] S.M.G. Yek, D. Azarifar, M. Nasrollahzadeh, M. Bagherzadeh, M. Shokouhimehr, *Separation and Purification Technology*, 247 (2020). 116952.
- [29] A. Balakrishnan, S. Appunni, M. Chinthala, M.M. Jacob, D.V.N. Vo, S.S. Reddy, E.S. Kunnel, *Environmental Chemistry Letters*, 1-25 (2023).
- [30] A. Bamoniri, B.B.F. Mirjalili, N. Moshtael-Arani, *Green Chemistry Letters and Reviews*, 7(4) (2014) 393-403.
- [31] N. Chouhan, R. Ameta, R.K. Meena, *Journal of Molecular Liquids*, 230 (2017) 74-84.
- [32] M. K. Guria, M. Majumdar, M. Bhattacharyya, *Journal of Molecular Liquids*, 222 (2016) 549-557.
- [33] P. Nariya, M. Das, F. Shukla, S. Thakore, *Journal of Molecular Liquids*, 300 (2020) 112279.
- [34] U. Sharma, N. Kumar, P. K. Verma, V. Kumar, B. Singh, *Green chemistry*, 14(8) (2012) 2289-2293.
- [35] U. Sharma, P.K. Verma, N. Kumar, V. Kumar, M. Bala, B. Singh, *Chemistry—A European Journal*, 17(21) (2011) 5903-5907.
- [36] N. Arora, A. Mehta, A. Mishra, S. Basu, *Applied Clay Science*, 151 (2018) 1-9.
- [37] H.L. Jiang, S.K. Singh, J.M. Yan, X.B. Zhang, Q. Xu, *Chemistry & Sustainability Energy & Materials*, 3(5) (2010) 541-549.
- [38] W.S. Hummers Jr, R.E. Offeman, *Journal of the American chemical society*, 80(6) (1958) 1339-1339.
- [39] H. Su, S. Wu, Z. Li, Q. Huo, J. Guan, Q. Kan, *Applied Organometallic Chemistry*, 29(7) (2015) 462-467.
- [40] K.O. Olumurewa, B. Olofinjana, O. Fasakin, M. A. Eleruja, E.O.B. Ajayi, *Graphene*, 6(4) (2017) 85-98.
- [41] Z. Li, S. Wu, H. Ding, D. Zheng, J. Hu, X. Wang, Q. Kan, *New Journal of Chemistry*, 37(5) (2013) 1561-1568.

- [42] L.H. Abdel-Rahman, N.M. Ismail, M. Ismael, A. M. Abu-Dief, E.A.H. Ahmed, *Journal of Molecular Structure*, 1134(2017) 851-862.
- [43] F. Adam, S.H. Abbas, *Journal of Physical Science*, 27(1) (2016) 15.
- [44] S.K. Gupta, C. Anjana, N. Sen, R.J. Butcher, J. P. Jasinski, J.A. Golen, *Polyhedron*, 89 (2015) 219-231.
- [45] A.M. Abu-Dief, R.M. El-Khatib, F. S. Aljohani, H.A. Al-Abdulkarim, S. Alzahrani, G. El-Sarrag, M. Ismael, *Computational Biology and Chemistry*, 97 (2022) 107643.
- [46] M.S. Asha, P. Othbert, M. V. N. Nagendra, R. Varadha Delarasoltanesmaeili., *Int. J. of Adv. Res.*, 4 (8) (2016) 1065-1074.
- [47] O.E. Sherif, N.S. Abdel-Kader, *Spectrochimica Acta Part A: Molecular and Biomolecular Spectroscopy*, 117 (2014) 519-526.
- [48] O.A.W. Handy, M.S.S. Jamil, M. Shamsuddin, *Mal. J. Fund. Appl. Sci.*, 16 (2020) 351-358.
- [49] W. Benabid, K. Ouari, S. Bendia, R. Bourzami, M.A. Ali, *Journal of Molecular Structure*, 1203 (2020) 127313.
- [50] H.M. Abd El-Lateef, A.D.M. Mohamad, M.R. Shehata, A.M. Abu-Dief, *Applied Organometallic Chemistry*, 36(7) (2022) e6718.
- [51] S. Ilhan, H. Temel, I. Yilmaz, M. Sekerci, *Journal of Organometallic Chemistry*, 692(18) (2007) 3855-3865.
- [52] A.A.M. Belal, I.M. El-Deen, N.Y. Farid, R. Zakaria, M.S. Refat, *Spectrochimica Acta Part A: Molecular and Biomolecular Spectroscopy*, 149 (2015) 771-787.
- [53] Z. Li, S. Wu, H. Ding, D. Zheng, J. Hu, X. Wang, Q. Kan, *New Journal of Chemistry*, 37(5) (2013) 1561-1568.
- [54] S. Kumari, A. Shekhar, D.D. Pathak, *RSC Advances*, 6(19) (2016) 15340-15344.
- [55] A. Allahresani, *Journal of the Iranian Chemical Society*, 14(5) (2017) 1051-1057.
- [56] L.H. Abdel-Rahman, M.T. Basha, B.S. Al-Farhan, M. R. Shehata, E.M. Abdalla, *Applied Organometallic Chemistry*, 36(1) (2022) e6484.
- [57] B.S. Creaven, B. Duff, D.A. Egan, K. Kavanagh, G. Rosair, V.R. Thangella, M. Walsh, *Inorganica Chimica Acta*, 363(14) (2010) 4048-4058.
- [58] L.H. Abdel-Rahman, A. M. Abu-Dief, R.M. El-Khatib, S.M. Abdel-Fatah, *Bioorganic chemistry*, 69 (2016) 140-152.
- [59] L.H. Abdel-Rahman, A.M. Abu-Dief, R.M. El-Khatib, S.M. Abdel-Fatah, *Journal of Photochemistry and Photobiology B: Biology*, 162 (2016) 298-308.
- [60] K.A. Wanderley, A.M. Leite, G. Cardoso, A. M. Medeiros, C.L. Matos, R.C. Dutra, Suarez, P. A. (2019). *Brazilian Journal of Chemical Engineering*, 36, 1165-1173.
- [61] H. Hassan, A. Tolba, E.S. El-Sharkawy, *Frontiers in Scientific Research and Technology*, 1(1) (2020) 57-67.
- [62] H.P. Mungse, S. Verma, N. Kumar, B. Sain, O. P. Khatri, *Journal of materials chemistry*, 22(12) (2012) 5427-5433.
- [63] H.M. Hassan, M.A. Betiha, E.A. El-Sharkawy, R.F. Elshaarawy, N.B. El-Assy, A.A. Essawy, A.M. Rabie, *Colloids and Surfaces A: Physicochemical and Engineering Aspects*, 591 (2020) 124520.
- [64] H. Su, S. Wu, Z. Li, Q. Huo, J. Guan, Q. Kan, *Applied Organometallic Chemistry*, 29(7) (2015) 462-467.
- [65] Z. Ghadamyari, A. Khojastehnezhad, S. M. Seyedi, F. Taghavi, A. Shiri, *ChemistrySelect*, 5(33) (2020) 10233-10242.
- [66] Z.H.O.U. Xue-Fei, Z.R. ZOU, X.J. Yang, *Rev. Roum. Chim.*, 65(11) (2020) 973-982.
- [67] A. Zarnegaryan, M. Moghadam, S. Tangestaninejad, V. Mirkhani, I. Mohammdpoor-Baltork, *New Journal of Chemistry*, 40(3) (2016) 2280-2286.
- [68] L. Qian, P. Liu, S. Shao, M. Wang, X. Zhan, S. Gao, *Chemical Engineering Journal*, 360 (2019) 54-63.
- [69] M.S. Dastjerdy, N. Monadi, *Applied Organometallic Chemistry*, 37(1) (2023) e6931.
- [70] S. Kujur, S. Verma, D.D. Pathak, *Catalysts*, 12(11) (2022) 1458.
- [71] P. Bhanja, S.K. Das, A.K. Patra, A. Bhaumik, *RSC advances*, 6(76) (2016) 72055-72068.
- [72] P. Liu, Y. Huang, L. Wang, *Materials Letters*, 91 (2013) 125-128.
- [73] S. Harish, J. Mathiyarasu, K.L.N. Phani, V.J.C.L. Yegnaraman, *Catalysis letters*, 128 (2009) 197-202.
- [74] W. Che, Y. Ni, Y. Zhang, & Y. Ma, *Journal of Physics and Chemistry of Solids*, 77 (2015) 1-7.
- [75] M. Nanaei, M.A. Nasserri, A. Allahresani, M. Kazemnejadi, *SN Applied Sciences*, 1 (2019) 1-12.
- [76] A. Iben Ayad, D. Luart, A. Ould Dris, E. Guénin, *Nanomaterials*, 10(6) (2020) 1169.
- [77] N. Pradhan, A. Pal, T. Pal, *Colloids and Surfaces A: Physicochemical and Engineering Aspects*, 196(2-3) (2002) 247-257.
- [78] K. Hasan, I.A. Shehadi, N.D. Al-Bab, A. Elgamouz, *Catalysts*, 9(10) (2019) 839.
- [79] S. Chen, Y. Xiang, C. Peng, W. Xu, M.K. Banks, R. Wu, *Inorganic Chemistry Frontiers*, 6(4) (2019) 903-913.
- [80] X.L. Liu, X. Yang, H.Y. Xin, X.P. Tang, L.J. Weng, Y.Y. Han, D. Geng, *Digest Journal of Nanomaterials & Biostructures (DJNB)* (2016) 11(2).
- [81] K. Hasan, I.A. Shehadi, N.D. Al-Bab, A. Elgamouz, *Catalysts*, 9(10) (2019) 839.
- [82] H.W. Garba, M.S. Abdullahi, M.S.S. Jamil, N.A. Endot, *Molecules*, 26(19) (2021) 5876.
- [83] N. Sahiner, H. Ozay, O. Ozay, N. Aktas, *Applied Catalysis A: General*, 385(1-2) (2010) 201-207.
- [84] B. Sreedhar, D.K. Devi, D.Yada, *Catalysis Communications*, 12(11) (2011) 1009-1014.
- [85] S. Bhar, R. Anandkrishnan, *RSC advances*, 5(27) (2015) 20704-20711.
- [86] J. Chen, H. Zhang, P. Liu, Y. Li, X. Liu, G. Li, H. Zhao, *Applied Catalysis B: Environmental*, 168 (2015) 266-273.
- [87] J. Albadi, H.A. Samimi, M. Jalali, *Acta Chimica Slovenica*, 66(3) (2019) 740-744.
- [88] Z. Duan, G. Ma, W. Zhang, *Bulletin of the Korean Chemical Society*, 33(12) (2012) 4003-4006.
- [89] J. Yang, X. Shen, G. Zhu, Z. Ji, H. Zhou, *RSC Advances*, 4(1) (2014) 386-394.